Missouri S&T Library and Learning Resources

Scholars' Mine

Masters Theses

Student Theses and Dissertations

Spring 2014

Theoretical analysis of shape separation of particles using flow field-flow fractionation

Mehrdad Alfi

Follow this and additional works at: https://scholarsmine.mst.edu/masters_theses

 Part of the Chemical Engineering Commons

Department:

Recommended Citation

Alfi, Mehrdad, "Theoretical analysis of shape separation of particles using flow field-flow fractionation" (2014). *Masters Theses*. 7262.
https://scholarsmine.mst.edu/masters_theses/7262

This thesis is brought to you by Scholars' Mine, a service of the Missouri S&T Library and Learning Resources. This work is protected by U. S. Copyright Law. Unauthorized use including reproduction for redistribution requires the permission of the copyright holder. For more information, please contact scholarsmine@mst.edu.

THEORETICAL ANALYSIS OF SHAPE SEPARATION OF PARTICLES USING FLOW FIELD-FLOW FRACTIONATION

by

MEHRDAD ALFI

A THESIS

Presented to the Faculty of the Graduate School of the

MISSOURI UNIVERSITY OF SCIENCE AND TECHNOLOGY

In Partial Fulfillment of the Requirements for the Degree

MASTER OF SCIENCE IN CHEMICAL ENGINEERING

2014

Approved by

Joontaek Park, Advisor
Gholamreza Zahedi
Manashi Nath
Xinhua Liang

PUBLICATION THESIS OPTION

This thesis consists of an article presented in Pages 7-28, that have been published in Journal of Separation Science. An appendix has been added for purposes normal to thesis writing.

ABSTRACT

Size separation of spherical and rod-like particles in Flow Field-flow Fractionation was investigated theoretically. The effect of cross flow migration and rod orientation was also investigated as a new mode of study. It has been shown that the rod local orientation makes different diffusivity values in comparison with spherical particles and helps particle separation. Additionally, a new mechanism of lift-hypelayer mode was used for rod-like particles which can be compared with steric mode of spherical particles. This mechanism is said to be due to hydrodynamic interaction of rod-like particle with wall and with other rods.

As a measure of axial and cross flow velocity, Peclet number was defined in each case with respect to spherical particle or rod-like particle. Based on different Peclet numbers, operations were divided into four different regions each with a dominant mode. Additionally, retention ratio of each particle category was calculated using concentration profile and velocity profile. Summing up all the effects, the conclusion was drawn that according to what size of particle to separate, one should choose proper axial and cross-flow velocity together with proper mode of operation.

Finally, based on theoretical studies, it was concluded that shape separation of rod-like particles is feasible for particles in micro size. However, for smaller particles experimental investigation may be needed.

ACKNOWLEDGMENTS

I would like to express my sincere gratitude to my advisor, Dr. Joontaek Park for giving me a novel, challenging project to work on. I have been amazingly fortunate to have an advisor who gave me the freedom to explore on my own and at the same time the guidance to recover when my steps faltered. Dr. Park taught me how to question thoughts and express ideas. His patience and support helped me overcome many crisis situations and finish this thesis. I hope that one day I would become as good an advisor to my students as Dr. Park has been to me. Hereby, I'm grateful to Dr. Gholamreza Zahedi, Dr. Manashi Nath and Dr. Xinhua Liang for consenting to serve on my graduate committee. Financial assistance from Department of Chemical and Biochemical Engineering is gratefully acknowledged.

Last but not the least, I would like to thank my family for all their love and encouragement. To my Mom and Dad who raised me with a love of science and supported me in all my pursuits. To my supportive beloved uncle, Abbas, for his constant inspiration. To my brother, Masoud, who is my best friend, he is the one who helped me overcome many challenging situations, and to my lovely sister, Mahshid, for her love and sweet emotional interests. This thesis would not be possible without the love and support of you dears.

TABLE OF CONTENTS

LIST OF ILLUSTRATIONS

Page

1. INTRODUCTION

1.1. NANORODS

Nanorods are a kind of morphology with length ranging from 1 to 100 nm and aspect ratio (length to diameter ratio) of 1.5 to 10 nm. They can be synthesized from either metallic or non-metallic materials. One of the most important applications of nanorods is in medical science. In this article, separation process for two major types of nanorods including Gold Nanorods (GNRs) and Carbon Nanotubes (CNTs) is investigated.

1.1.1. Gold Nanorods (GNRs). Gold Nanorods are important mostly due to their optical properties. Rod-like nanoparticles of Au can be synthesized in a variety of techniques each with specific advantages among which, the most popular is seed mediated growth. In every synthesis technique, there always been unreacted materials and impurities. As an example, while producing gold nanorods from spherical particles, the product may be a combination of rods and spheres which needs to be separated. So, separation techniques play an important role in nanoparticle science.

1.1.2. Carbon Nanotubes (CNTs). These kind of cylindrical nanostructures are formed by the means of rolling very thin carbon sheets (thickness of an atom) called graphene. Carbon nanotubes based on number of sheets rolled together concentrically, are categorized to single-walled and multi-walled carbon nanotubes. There are number of methods for synthesizing CNTs, like Arc Discharge, Chemical Vapor Deposition (CVD) and laser ablation. Based on the synthesis method, various shapes and sizes of CNTs are formed which need to be purified in order to be applicable.

1.2. FLOW FIELD FRACTIONATION

Flow Field Fractionation (FFF) is a versatile flow-based separation technique. Basis of this technique is on difference in diffusion coefficient of various particles inside a suspension and force balance corresponding to each particle. In this method, a suspension of samples is injected to a thin channel to pass in thoroughly. Meanwhile, another field perpendicular to fluid flow is applied to the channel effecting particle's distance from the channel wall. The applied field can be a fluid flow, electrical field, magnetic field or temperature gradient (thermal field).

During past decades, there has been a growing interest on separation of rod-like particles using FFF. Application of asymmetric-flow field flow fractionation (A4F) were investigated by Gigault et al. [1]. In their work, A4F was used in order to fractionate positively charged particles and as a result, an optimized condition for carrier fluid was determined. Application of asymmetrical flow FFF was also conducted by Runyon et al. [2] for size (and shape) separation of nanorods. In this work, diffusion equations of Aragon and Flamik for cylinders were used as an estimation for hydrodynamic characteristics of nanorods for a variety of sizes and aspect ratios. This kind of FFF method has been extensively used for separation of other cylinder-shaped particles like single-wall carbon nanotubes (SWCNT) and multi-wall carbon nanotubes (MWCNT) [3-5]. As another method for separation of rod-like particles, one can name flow field-flow fractionation. Chun et al. [6] used flow field-flow fractionation for separation of single-wall carbon nanotubes suspended in aqueous dispersions. Then, they compared effectiveness of FFF separation with that of size exclusion chromatography (SEC) at constant pre-defined "hydrodynamic length" characteristic. Applying both slender body

theory and prolonged ellipsoid theories, they concluded that the slender body theory is a stronger theory for approximation of dynamics of SWCNTs. Giddings et al. [7] used flow FFF for separation of DNA chain molecules. They have maintained use of different FFF techniques by subject. As for DNA example, molecules with same weight but different shapes (circular, linear or different in number of superhelical turns) cannot be eluted using sedimentation FFF. Instead, because of difference in hydrodynamic diameter and diffusion coefficient, flow FFF is a strong tool in this case. On the other hand, for molecules with the same shape and different weight, flow FFF is not useful and one should use sedimentation FFF. Accordingly, they focused on acquiring diffusivity measures using flow FFF. As a result, they concluded first, the accurateness of diffusivity coefficients measured by flow FFF and secondly, highly dependency of D coefficient on channel thickness. Chen et al. [8] on the other hand, focused on differences between SWCNT and MWCNT separation in flow FFF. They fractionated SWCNTs in normal mode and MWCNTs in steric mode. As a conclusion, logarithmic relation between retention volume and carbon nanotube length is a linear one for SWCNTs and nonlinear for MWCNTs. While in case of MWCNT fractionation is affected by parameters like diameter and rigidity, by increasing particle length the effect of length becomes dominant.

1.3. SHAPE SEPARATION

Synthesis of nanoparticles can lead to a wide variety of particle shapes each with different properties. These kinds of nanoparticles are never totally monodisperse, which makes them unable to be applicable directly in many cases. As an example of shape and

size dependent of properties, one can mention cytotoxicity of gold nanoparticles in which certain sizes of gold nanoparticles can cause toxicity in cellules and organisms [9, 10].

1.3.1. Chromatography. This method is similar to FFF technique based on having a mobile phase containing mixtures and fractionation based on particles mobility. One particular type of chromatography which is used for size and shape separation is called Size Exclusion Chromatography (SEC). Basis of this technique is on difference in particle's hydrodynamic volume. While mobile phase is moving through porous media, small particles can pass stationary phase easily and then elute slowly. On the other hand, larger particles go through accessible volume and elute faster. Al-Somali et al. [11, 12] used a new technique of Recycling Size Exclusion Chromatography (RSEC) as a strong technique for high resolution separation of materials based on size. In comparison with traditional closed-loop techniques, they have shown that RSEC have better efficiency and is capable of separating nanocrystals with only 6 Å difference in size.

1.3.2. Magnetic Field Separation. Nanoparticles can be separated based on magnetic susceptibilities and size. This method can be used mainly for particles with size more than 50 nm. At lower sizes, contribution of thermal diffusion and Brownian forces on particle, makes this method almost inapplicable [13]. Yavuz et al. [14] used low magnetic field gradient (<100 T/m) in order to separate differently sized magnetite (Fe3O4) particles. They showed that this happens because of high field gradient present as surface of nanoparticles. Rheinländer et al. [15] on the other hand, compared fractionation of magnetic particles using Magnetic Fractionation (MF) with Size Exclusion Chromatography (SEC). They got almost similar results for fractionation of

nanoparticles using each technique but concluded that MF is a strong technique for optimizing magnetic fluids regarding their application.

1.3.3. Electrophoresis. This method is based on migration of charged particles towards opposite-polarity electrode in an electric field. Dominating force affecting particles in this method is the force by electrophoretic mobility, which depends on applied field, and frictional forces which depend on particle shape and size (this is the basis of using this method for shape separation). There are three major categories of electrophoresis, which are Gel Electrophoresis (GE), Free Flow Electrophoresis (FFE), and Isoelectric Focusing (IEF) electrophoresis. Hanauer et al. [16] used agarose gel electrophoresis to separate rod-like particles of gold and silver from spherical and triangular particles. In order to functionalize particles for this technique, they coated particles with a charged layer of polyethylene glycol. They used Henry formula and the Gouy-Chapman and measured a clear separation of same-size silver particles.

References

1. Gigault, J., T. J. Cho, R. I. MacCuspie and V. A. Hackley, Gold nanorod separation and characterization by asymmetric-flow field flow fractionation with UV–Vis detection. Analytical and bioanalytical chemistry, 2013. **405**(4): p. 1191-1202.

2. Runyon, J.R., A. Goering, K. T. Yong and S. K. Williams, Preparation of Narrow Dispersity Gold Nanorods by Asymmetrical Flow Field-Flow Fractionation and Investigation of Surface Plasmon Resonance. Analytical Chemistry, 2012. **85**(2): p. 940-948.

3. Gigault, J., B. Grassl, and G. Lespes, *Multi-wall carbon nanotube aqueous dispersion monitoring by using A4F-UV-MALS.* Analytical and bioanalytical chemistry, 2011. **401**(10): p. 3345-3353.

4. Gigault, J., I. L. Hécho, S. Dubascoux, M. Potin-Gautier and G. Lespes, Single walled carbon nanotube length determination by asymmetrical-flow field-flow fractionation hyphenated to multi-angle laser-light scattering. Journal of Chromatography A, 2010. **1217**(50): p. 7891-7897.

5. Cho, T.J. and V.A. Hackley, Fractionation and characterization of gold nanoparticles in aqueous solution: asymmetric-flow field flow fractionation with MALS, DLS, and UV–Vis detection. Analytical and bioanalytical chemistry, 2010. **398**(5): p. 2003-2018.

6. Chun, J., J. A. Fagan , E. K. Hobbie and B. J. Bauer, Size separation of single-wall carbon nanotubes by flow-field flow fractionation. Analytical chemistry, 2008. **80**(7): p. 2514-2523.

7. Liu, M.K. and J.C. Giddings, Separation and measurement of diffusion coefficients of linear and circular DNAs by flow field-flow fractionation. Macromolecules, 1993. **26**(14): p. 3576-3588.

8. Chen, B. and J.P. Selegue, Separation and Characterization of Single-Walled and Multiwalled Carbon Nanotubes by Using Flow Field-Flow Fractionation. Analytical Chemistry, 2002. **74**(18): p. 4774-4780.

9. Jiang, W., B. Y. S. Kim, J. T. Rutka and W. C. W. Chan, Nanoparticle-mediated cellular response is size-dependent. Nat Nano, 2008. **3**(3): p. 145-150.

10. Pan, Y., S. Neuss, A. Leifert, M. Fischler, F. Wen, U. Simon, G. Schmid, W. Brandau and W. Jahnen-Dechent, *Size-dependent cytotoxicity of gold nanoparticles.* Small, 2007. **3**(11): p. 1941-9.

11. Al-Somali, A.M., K. M. Krueger, J. C. Falkner and V. L. Colvin, Recycling size exclusion chromatography for the analysis and separation of nanocrystalline gold. Anal Chem, 2004. **76**(19): p. 5903-10.

12. Krueger, K.M., A. M. Al-Somali, J. C. Falkner and V. L. Colvin, Characterization of nanocrystalline CdSe by size exclusion chromatography. Anal Chem, 2005. **77**(11): p. 3511-5.

13. Fletcher, D., *Fine particle high gradient magnetic entrapment.* Magnetics, IEEE Transactions on, 1991. **27**(4): p. 3655-3677.

14. Yavuz, C.T., J. T. Mayo, W. W. Yu, A. Prakash, J. C. Falkner, S. Yean, L. Cong, H. J. Shipley, A. Kan, M. Tomson, D. Natelson and V. L. Colvin, Low-Field Magnetic Separation of Monodisperse Fe3O4 Nanocrystals. Science, 2006. **314**(5801): p. 964-967.

15. Rheinländer, T., et al., *Different methods for the fractionation of magnetic fluids.* Colloid and Polymer Science, 2000. **278**(3): p. 259-263.

16. Hanauer, M., S. Pierrat , I. Zins, A. Lotz and C. Sönnichsen, Separation of Nanoparticles by Gel Electrophoresis According to Size and Shape. Nano Letters, 2007. **7**(9): p. 2881-2885.

PAPER

Theoretical analysis of the local orientation effect and the lift-hyperlayer mode of rod-like particles in field-flow fractionation

Abstract: We investigated theoretically the effects of the cross-stream migration and the local average orientation of rodlike particles on the shape-based separation using field-flow fractionation. The separation behavior was analyzed by comparing the retention ratios of spheres and rods. The retention ratio of a rod was evaluated through the derivation of its cross-sectional concentration profile by considering the rod migration and the local average orientation. Our study in various flow conditions showed that the rod migration, caused by the hydrodynamic interaction with a wall, can affect the separation behavior as a lift-hyperlayer mode. We also demonstrated that the local average orientation, which is a function of a local shear rate and a rotational diffusivity, results in the transverse diffusivity which is different from its perpendicular diffusivity. These results suggest that the experimental separation behaviors of rods in field-flow fractionation may not be fully explained by the current theory based on the normal mode and the steric mode. We also characterized each condition where one of the normal mode, the steric mode of spheres, and the lift-hyperlayer mode of rods is dominant.

Keywords: field flow fractionation, lift-hyperlayer mode, hydrodynamic interaction, particle shape separation, slender body, rodlike particles

1. INTRODUCTION

As an increasing number of studies on the application of rodlike nanoparticles, such as single walled carbon nanotubes (SWNTs) or gold nanorods (GNR), have been performed, various methods for producing these nanorods have also been developed [1,2]. As the desired physical properties of nanorods are usually dependent on their shapes, there has been growing attention on the development of shape-based separation or characterization methods for rodlike particles. Various methods, such as self-assembly [3], centrifuge, chromatography and electrophoresis (references herein [4]), have been proposed for GNR shape separation. However, in this study, we are especially interested in the theoretical investigation of the shape separation of rods from spherical particles utilizing field-flow fractionation (FFF) [5].

A fundamental principle of the FFF separation is demonstrated in Fig. 1.A. While a particle mixture is flowing in the axial flow in the FFF channel, the cross force pushes the particles towards the bottom of the channel ("accumulation wall"). However, the cross force encounters an opposing force so that the particles can be distributed further away from the wall. Since the axial flow has a parabolic velocity profile, the particles with the stronger opposing force tend to be distributed in a higher velocity region, which results in the faster elution [5]. Therefore, the desired particle separation using FFF requires the careful selection of the type of the cross force field and the "mode" of the opposing force. In this study, we focus only on the Flow-FFF (Fl-FFF) where a cross flow is used as a cross force field. As the opposing forces, we do not consider only the normal mode and the steric mode, as in the previous studies, but also the lift-hyperlayer mode.

The "normal mode", which is a basic mechanism in the size separation, can be used in the shape separation. Assuming that a particle is spherical and its concentration is dilute, a smaller particle has a larger isotropic diffusivity (a stronger opposing Brownian force) by the Stokes-Einstein equation,

$$D_o = \frac{k_B T}{6\pi\mu r_o} \quad (1)$$

(D_O is a diffusivity of the sphere, k_B is the Boltzmann's constant, T is an absolute temperature, μ is the solvent viscosity, and r_o is the sphere radius). Therefore, non-spherical particles are usually assumed as spheres with the same volume. However, if a particle shape is radically different from a sphere, its anisotropic diffusivity must be considered. It can be assumed that a non-spherical particle still behaves like a sphere with D_O as long as the value of its diffusivity in the transverse direction, D_X, equals D_O, as demonstrated in Fig. 1.B. Under this assumption, the size of a non-spherical particle can be characterized by the equivalent radius, r_{eq}, which is the radius of a spherical particle with D_O=D_X. Equating Eq. (1) with D_X will obtain the relation between r_{eq} and D_X,

$$r_{eq} = \frac{k_B T}{6\pi\mu D_X} \quad (2)$$

Therefore, the relation between the elution time and r_{eq} for the normal mode FFF would be also a monotonically increasing function. This also implies that particles with different shapes can be separated by the normal mode FFF as long as they have different r_{eq}. For example, this principle was applied to SWNT separation using asymmetrical Fl-FFF (A4F) [6]. Chun *et al.* [7] characterized SWNTs according to their lengths by comparing the elution times of each fraction of SWNTs with those of spherical particles with known sizes.

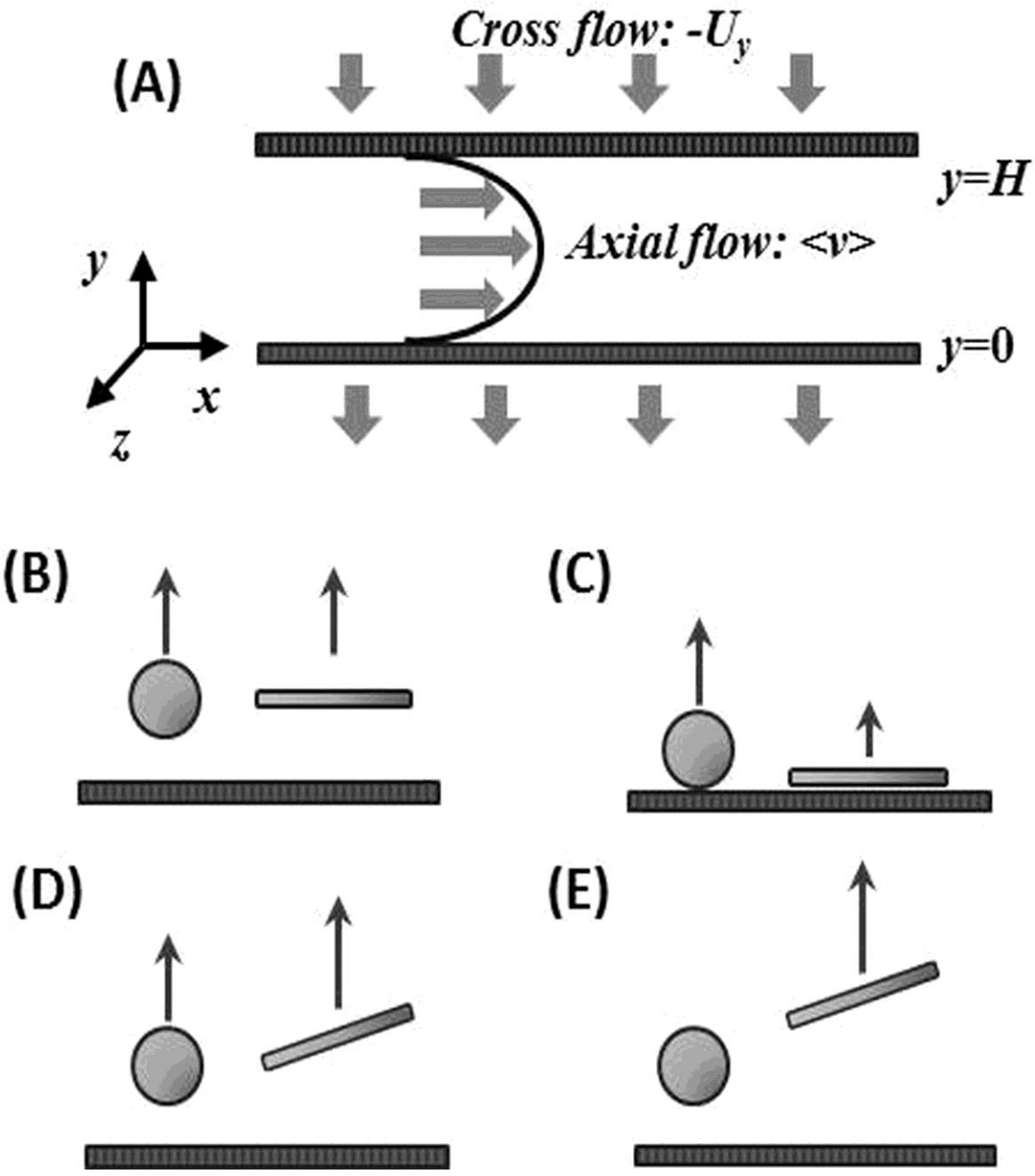

Figure 1. A) schematic diagram of a Flow-FFF channel and spheres/rods with $D_0=D_\perp$ in different operating modes B) the normal mode with a rod aligned in the axial flow direction, C) the steric mode, D) the normal mode with a rod with Brownian rotation, and E) the lift-hyperlayer mode. The arrows on the particles represent the opposing forces in each mode.

The “steric mode” is also important in shape separation. When the cross flow is strong enough to suppress the diffusion, particles flow almost on the wall surface. Therefore, a particle of which configuration enables closer location to the wall is eluted later. It was shown that there exists a condition where the elution order of sphere size becomes reversed in a graph for the elution time and r_o [5]. However, a simulation by Phelan and Bauer [8] has shown that the trend for the relation between elution time and r_{eq} of rodlike particles does not show the steric inversion as in that of spheres with r_o=r_{eq}. This is because the possible configuration on the wall is different according to the shape. For example, as shown in Fig. 1.C, a rod in an axial flow with high velocity is aligned near the surface so that the closest possible position from the wall is one half of the rod diameter, d/2, which is much smaller than r_o=r_{eq}. Note here that Beckett and Giddings [9] also performed a more rigorous analysis on the rod steric effect.

As we have reviewed, the normal mode and the steric mode have been applied to the shape separation so far. The recent works using A4F [4,10,11] reported the successful separation of gold nanorods by aspect ratio, A=L/d (a ratio between a rod length and a diameter) using A4F. However, there still exist experimental results, such as the elution order according to A, which are not clearly explained by the current theory based on the normal mode and the steric mode [10]. The motivation of this work is to advance the theory for the shape separation in FFF by considering the differences in particle dynamics according to shape in a more rigorous way. Our analysis includes the local average orientation and the transverse migration of rodlike particles, which are not considered in the previous works [7-9].

The concept of the local average orientation of non-spherical particles was introduced to the FFF analysis by Gajdos and Brenner [12]. However, it has rarely been applied in later studies. Chun [7] as well as Phelan and Bauer [8] chose the value of D_X of a rod as its perpendicular diffusivity, $D_\perp$, which is for the diffusion in a perpendicular direction to its principal axis. They assumed that a rod is aligned in the axial flow direction and D_X is constant as $D_\perp$ under a low retention time condition. However, it has been shown that Brownian rotation of a rod makes its orientation not perfectly aligned in shear flows and results in the average orientation being dependent on the shear rate [13-15]. Moreover, the shear rate,$\dot{\gamma}$, in the parabolic flow is dependent on the *x*-position. Consequently, D_X of a rod is not equal to $D_\perp$, nor constant in the transverse direction. Therefore, we evaluated D_X as a function of position by considering the local average orientation of a rod, as demonstrated in Fig. 1.D, to include this effect in our analysis.

We also included the transverse migration effect, as another opposing force, to consider the "lift-hyperlayer mode", as in Fig. 1.E. Based on rod migration theory [16-18], the hydrodynamic interaction between a rod and a wall can induce transverse motion of a rod in some conditions. Since this mechanism is unique to rods, not to spheres, identifying the condition to affect the separation behavior can be applied to shape separation. It is noteworthy that Chun [7] referred to only a minor effect of the hydrodynamic interaction [19], compared to the migration theory [16-18] developed further, for justification of the rod alignment.

We will demonstrate how to evaluate the concentration profile of rods considering the local orientation and the migration. Using the profile, the retention ratios of rods/spheres will be evaluated to discuss the feasibility of the shape separation.

2. THEORY & NUMERICAL METHODS

2.1. CONCENTRATION PROFILE

In this section, we will demonstrate how to derive the concentration profile of rodlike particles for each mode of the opposing forces. As shown in Fig. 1.A, there is a rectangular FFF channel with its thickness, *w*, and its breadth, *B*. Here, we set a coordinate system such that the axial flow direction is the *y*-direction, and the cross field is applied in the negative *x*-direction. The accumulation wall surface is set as x=0 and the opposite wall as x=w. It is assumed that B>>w to neglect the z-direction effect. It is also assumed that the flow is Newtonian and in the Stokes-flow region. Note here that we only derive the steady state concentration profile by considering only the effect in the *x*-direction. Therefore, the peak dispersion will be considered in our future work.

It was shown that the concentration profile of a solute in the transverse direction, $c(x)$, can be derived by balancing the cross force and the opposing force [5]. For the normal mode of Fl-FFF, the flux of a particle in the *x*-direction, J_x, can be expressed with:

$$J_x = -U_x c(x) - D_X \frac{dc(x)}{dx} \tag{3}$$

Here, the first term on the right hand side represents the cross flow effect with a flow rate of U_x and the second term describes the opposing Brownian force with D_X. When those two forces are balanced, the flux becomes 0 and the concentration profile reaches a steady state. The steady state $c(x)$ can be obtained by solving Eq. (3) for J_x=0:

$$\mathrm{c}(x) = c_o exp\left(-\frac{xU_x}{D_X}\right) \tag{4}$$

Here, c_o is the particle concentration at the accumulation wall. It is noteworthy that Eq. (3) has an underlying assumption that the particle has a constant D_X over the whole *x*-

position. However, the diffusivity of a non-spherical particle is in a tensor form which can describe the dependency on its configuration, which is also determined by $\dot{\gamma}$ and the Brownian rotation.

The *x*-position dependency of the configuration of the non-spherical particle, consequently D_X, in FFF is due to the parabolic velocity profile of the axial flow field, $v(x)$, which can be expressed as:

$$\mathrm{v}(x) = 6\langle v\rangle\left[\frac{x}{w} - \left(\frac{x}{w}\right)^2\right] \tag{5}$$

Here, <…> indicates an average over the cross section.

$$\langle \dots \rangle = \frac{1}{w}\int_0^w \dots dx \tag{6}$$

The position-dependent $\dot{\gamma}$ can be obtained by differentiating $v(x)$ over x:

$$\dot{\gamma} = \frac{\partial v(x)}{\partial x} = \frac{6\langle v\rangle}{w}\left[1 - \frac{2x}{w}\right] \tag{7}$$

In this study, we investigated the effect of the rod orientation, which is dependent on the *x*-position, on D_X and the resulting $c(x)$. To model a rodlike particle, we used a slender-body theory [20]. Assuming that A is high enough, its diffusivity can be approximated as the following tensor form:

$$\mathbf{D} = \frac{k_B T}{\xi}(\mathbf{I} + \mathbf{pp}) \tag{8}$$

(**D** is a diffusivity tensor, $\xi = \frac{4\pi\mu L}{\ln(2A)}$ is a resistance coefficient for a slender body, **I** is an identity tensor, and **p** is a unit vector of a rod orientation). It was [12,16-18] assumed that the rotational motion reaches its equilibrium much faster than that of the transverse diffusion. Therefore, the local diffusivity values at each *x*-position can be obtained by taking the orientation average of **D**. Since we do not consider the peak dispersion effect,

the component of **D** in Eq. (8), which affects $c(x)$, is $1+p_x^2$, where p_x is the x-component of **p**. Taking the orientation average of the effective component of **D**, the flux balance in the x-direction for a rod can be written as

$$J_x = -U_x c(x) - \frac{k_B T}{\xi}(1+\ll {p_x}^2 \gg)\frac{dc(x)}{dx} \tag{9}$$

Here, <<…>> is an orientation average using the orientation probability distribution function, φ,

$$\ll \cdots \gg = \int \ldots \varphi d\mathbf{p} \tag{10}$$

The expression for the steady state $c(x)$ of a rod considering its local average orientation can be obtained by solving Eq. (9) with J_x=0.

$$\mathrm{c}(x) = c_o exp\left(\int_0^x \frac{-U_y \xi / k_B T}{1+\ll {p_x}^2 \gg} d\bar{x}\right) \tag{11}$$

Here, $\bar{x}$ is a dummy variable for the integration. Due to the position-dependent $\dot{\gamma}$, as in Eq. (7), the average orientation moment $<<p_x^2>>$ is not constant but also a function of x-position. Therefore, the integration in Eq. (11) requires the evaluation of $<<p_x^2>>$ in each position.

Park [16-18] performed a Brownian dynamics simulation to evaluate the average orientation moments as a function of the Peclet number for 'shear' flow in the axial direction, Pe_S, which is defined as

$$Pe_S = \frac{\xi \dot{\gamma} L^2}{k_B T} = \frac{\dot{\gamma} L^2}{D_\perp} \tag{12}$$

The results were almost identical to the results from another approach by deriving φ [14,15]. Using Eq. (7) and Eq. (12), the average orientation moment as a function of

Pe_S can be converted into a function of the x-position. The converted results for an example case are shown in Fig. 2.

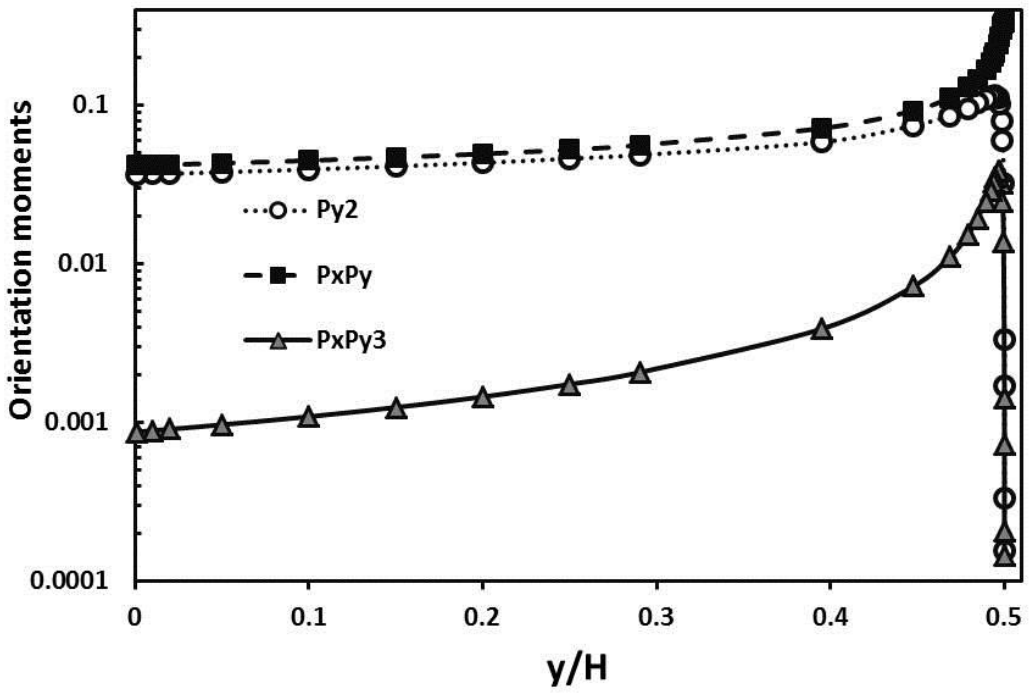

Figure 2. The orientation moments as a function of x/w in a Fl-FFF channel for the condition of r_{eq}=1 μm, A=100 as in Fig. 3.C.

In previous works by Chun [7] and Bauer and Phelan [8], the configuration of a rod was assumed to be aligned only in the axial flow direction so that $D_X=D_\perp$. In that case, $<<p_x^2>>$ becomes 0 and Eq. (11) turns back to Eq. (4). Although they also assumed that most of particles exist near the accumulation wall, Fig. 2 shows that $<<p_x^2>>$ still has non-zero and the x-dependent values.

According to the rod migration theory [16-18], for a Brownian rod under a shear flow near a wall, the coupling of the average orientation and the hydrodynamic interaction with a wall results in the rod migration away from a wall. This phenomenon was observed experimentally [21] as well as numerically [22]. To include the transverse migration effect in $c(x)$, the rod migration velocity, [16-18], was added to Eq. (9).

$$J_x = -U_x c(x) - \frac{k_B T}{\xi}(1+\ll {p_x}^2 \gg)\frac{dc(x)}{dx} + c(x)\frac{k_B T}{\xi}(\ll \mathrm{K} \gg + \ll \Gamma \gg) \qquad (13)$$

Here, <<K>> represents the migration due to hydrodynamic interaction with a wall. The detailed expression of this term is given as:

$$\ll \mathrm{K} \gg = \frac{L}{128\ln(2A)}\left[\frac{1}{x^2} - \frac{1}{(x-w)^2}\right]\left[Pe_S\left(\ll p_x p_y \gg -3 \ll p_y {p_x}^3 \gg\right)\right.$$
$$\left. + 72(1 - 3 \ll {p_x}^2 \gg)\right] \qquad (14)$$

Note here that there are other average orientation moments $<<p_x p_y>>$ and $<<p_y {p_x}^3>>$ in Eq. (14), of which the x-position dependency are also demonstrated in Fig. 2.

Additionally, <<Γ>> is given by:

$$\ll \Gamma \gg = -\frac{\partial \ll {p_x}^2 \gg}{\partial \mathrm{x}} \qquad (15)$$

This term is related to a migration due to the anisotropic diffusivity effect, which makes a Brownian rod migrate from a low shear region (the center of the channel) to a high shear region (near a wall) [23,24]. As in the Eq. (9)~(11), Eq. (13) can be solved for the no flux condition to get the expression for $c(x)$ considering both the migration and the local average orientation.

$$\mathrm{c}(x) = c_o exp\left(\int_0^x \frac{\left(-U_y \xi / k_B T\right) + \ll \mathrm{K} \gg + \ll \Gamma \gg}{1+\ll {p_x}^2 \gg} d\bar{x}\right) \qquad (16)$$

2.2. NUMERICAL INTEGRATION

To get $c(x)$ using Eq. (11) or (16) by integration, the average orientation moments should be identified as functions of the x-position as in Fig. 2. Although the asymptotic expressions for low and high Pe_S limits were also derived [16-18], analytical expressions for the intermediate Pe_S region ($240< Pe_S <12000$) of the orientation moments are not available yet. Therefore, the desired orientation moments should be estimated by linear interpolation using the results from their Brownian dynamics simulation [16-18].

The numerical integration of Eq. (16) was performed by the trapezoidal rule. For each integration point, a shear rate at that point was evaluated to be converted to local Pe_S using Eq. (12). The integration was actually performed over the range between $d/2$ and $w-d/2$, instead of 0 and w, in order to consider the steric effect by excluding the region where rigid particles cannot be located. The same concept was used by Giddings [25]. Additionally, the value of $c(x=d/2)$ cannot be directly evaluated by Eq. (16) because the integration becomes 0. Therefore, $c(x=d/2)$ is estimated by extrapolation using $c(x=d/2+\Delta x)$ and $c(x=d/2+2\Delta x)$, where Δx is the integration point interval and its value was set as smaller than $d/2$ to give convergent results.

The integration constant c_0 corresponds to the wall concentration for normal mode [5]. However, the wall concentration is not given for our analysis. Therefore, $c(x)$, is now modified as a probability distribution for the center of mass, $c^*(x)=c(x)/c_0$, by estimating c_0 as:

$$c_0 = \int_{d/2}^{w-d/2} c(x)dx \tag{17}$$

For convenience, the symbol * which indicates the center of mass distribution is dropped for the rest of this paper. From this point on, $c(x)$ is the center of mass probability distribution function.

We also used the following parameters: w=250 μm, T=293K, μ=0.001Pa.s, and the fluid density, ρ=1000kg/m^3.

2.3. RETENTION RATIO

The separation capability can be characterized by a variable, called as retention ratio, R, which is defined by:

$$\mathrm{R} = \frac{\langle c(x)v(x)\rangle}{\langle c(x)\rangle\langle v(x)\rangle} \tag{18}$$

The physical meaning of R is the ratio between the average flow rate of the eluting liquid and the solutes. For R~1, particles flow with the same velocity with $\langle v \rangle$ while R=0 means no elution from FFF. The evaluation of R from Eq. (18) can be performed by using Eq. (5) as well as $c(x)$ either from Eq. (4), Eq. (11) or Eq. (16), which can be chosen based on the types of particles: Equation (4) is used to obtain R_S, defined as R for a sphere. Equation (16) must be chosen to obtain R_M, defined as R for a rod considering the migration effect. Equation (11) can be used to obtain R_R, defined as R for a rod without considering the migration effect. The difference between R_M and R_R can be used for indicating the emergence of the lift-hyperlayer mode. For example, if there is a difference between R_M and R_R, the migration effect becomes dominant over normal mode. R_S also can be obtained analytically by using the expression for the steric mode of spheres, derived by Giddings [25].

$$R_s = 6(\alpha - \alpha^2) + 6\lambda(1-2\alpha)\left[\coth\left(\frac{1-2\alpha}{2\lambda}\right) - \frac{2\lambda}{1-2\alpha}\right] \quad (19)$$

Here, $\alpha = r_{eq}/w$ and $\lambda = D_O/(wU_x)$.

The errors between the results from the numerical integration of Eq. (18), with Eq. (4) and Eq. (17), and from Eq. (19) were less than 0.1%. In this study, R_S from Eq. (19) is used for comparison with R_M.

3. RESULTS

We calculated R_S, R_M and R_R as a function of r_{eq} with varying A, U_x, and a Peclet number in terms of the 'axial' flow rate, $Pe_X = \langle v \rangle L/D_\perp$ to investigate how the rod orientation and the rod migration make a difference between spherical and rodlike particles with the same diffusivities, $D_o = D_\perp$. Since we chose to use Eq. (8) as the expression for the rod diffusivity, the particles with the same diffusivity condition can be written as:

$$D_o = \frac{k_B T}{6\pi\mu r_{eq}} = \frac{k_B T \ln(2A)}{4\pi\mu L} = D_\perp \quad (20)$$

For each r_{eq}, the rod lengths, L, both for A=10 and A=100 were calculated using the Eq. (20) so that the effect of A would also be investigated. Based on the rod migration analysis [16-18], the rod migration becomes obvious at high flow rates of Pe_S >1200. The effect of the axial flow rate on the lift-hyperlayer mode of rods was investigated for the conditions of Pe_X =12000 and 60000. The values of $\langle v \rangle$ and r_{eq} were selected for the chosen Pe_X as well as for satisfying the Stokes-flow condition ($\frac{2\rho\langle v \rangle r_{eq}}{\mu} < 0.1$). As indicated by Giddings, Eq. (19) shows the steric inversion as the r_{eq} increases. Hence, we

chose two values of U_x: U_x=5×10^{-8} m/s and U_x=5×10^{-7} m/s for a normal and a steric mode dominant condition, respectively. The results are shown in Fig. 3.

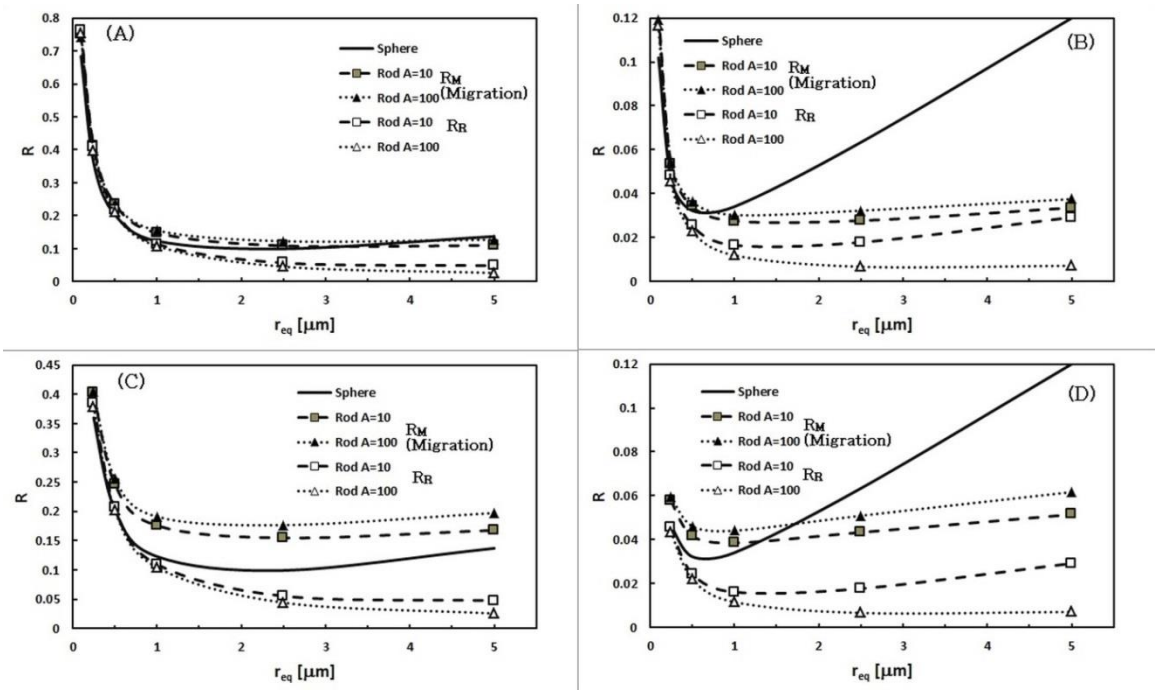

Figure 3. Comparison of R values as a function of r_{eq}. A) Pe_X=12000, U_x=5×10^{-8} m/s, B) Pe_X=12000, U_x=5×10^{-7} m/s,
C) Pe_X=60000, U_x=5×10^{-8} m/s, and D) Pe_X=60000, U_x=5×10^{-7} m/s.

Figure 3.A shows the results from the condition of Pe_X=12000 and U_x=5×10^{-8} m/s. As the r_{eq} increases, R_S decreases until r_{eq}=2.5 μm and slightly increases again at r_{eq}=5 μm due to the steric inversion. The retention ratios of rods also decrease with increasing r_{eq}. For the particles of r_{eq}<0.5 μm, all the retention ratios of rods are similar but their actual values are slightly larger than R_S (the difference is not clearly seen in the figure). An explanation of this is that the rod migration effect is not strong but the

orientation effect causes non-zero $<<p_x^2>>$ to make D_X slightly larger than $D_\perp$. For the particles of r_{eq}>0.5μm, the difference between R_M and R_R becomes larger with increasing r_{eq}. This indicates that the lift-hyperlayer becomes more obvious in that range of r_{eq}. The difference between R_S and R_R is due to the difference in the steric effect, as discussed by Phelan and Bauer [8]. However, the similar R_M and R_S are explained by comparison of $c(x)$ in Fig. 4.A. The maximum value of $c(x)$ of rods is located at a similar position ($x=r_{eq}$) of the maximum value of $c(x)$ of spheres because the rod can only migrate as much as the distance of r_{eq} in this condition. The stronger migration effect at larger r_{eq} can be explained in terms of the migration coefficient $L/\ln(2A)$ in the migration term, Eq. (14) and $<Pe_S>$, the mean Pe_S, which can be derived using Eq. (10) and Eq. (12):

$$\langle Pe_S \rangle = \frac{\langle|\dot{\gamma}|\rangle L^2}{D_\perp} = \frac{6\langle v \rangle L^2}{wD_\perp} \tag{21}$$

As r_{eq} increases while maintaining the same $D_\perp$ and A, L also gets larger resulting in an increase of $<Pe_S>$ as well as the migration coefficient. Additionally, the migration coefficient also explains why the effect of A on the R_M is found to be weak: An increase of A with the same $D_\perp$ increases L but the term $\ln(2A)$ in the denominator also increases slightly.

Figure 3.C shows the results from the condition of Pe_X=60000 and $U_x=5\times10^{-8}$ m/s. Since only the values of $<v>$ were increased from the previous condition of Fig. 3.A, the stronger effect of the rod migration can be observed: The gap between R_M and R_R becomes much larger because $<<p_x^2>>$ becomes smaller to decrease R_R and rods migrate further away from the wall so that R_M value exceeds R_S (Fig. 4.A). Interestingly, we can find a "lift" inversion point around r_{eq}~2 μm where rods with larger r_{eq} can be eluted

faster in the condition since this inversion is due to the lift-hyperlayer mode not steric mode.

Figure 3.B shows the results from the condition of Pe_X=12000 and U_x=5×10^{-7} m/s. Increased U_x results in the trend of the steric mode where R_S increases with increasing r_{eq} after the inversion around r_{eq}=0.5 μm. As in the case of Fig. 3.A, the retention ratios of rods were all similar for r_{eq}<0.2 μm and show a slight lift-hyperlayer mode for r_{eq} >0.2 μm. However, the migration effect is not enough to push the rods away from the wall as much as the steric exclusion of spheres from the wall. It is interesting to note that even the steric inversion of the rod with A=10 is observed around r_{eq}=1 μm.

Figure 3.D shows the results from the condition of Pe_X=60000 and U_x=5×10^{-7} m/s. Increased Pe_X results in the increased R_M as well as the lift inversion around r_{eq}=1 μm. For r_{eq}<1.5 μm, the lift-hyperlayer mode slightly prevails over the steric mode. However, the steric mode becomes much stronger than the migration effect at r_{eq}>1.5 μm (Fig. 4.B). We also note that the anisotropic diffusivity migration [23,24] was not observed in the conditions of this study, where most particles are distributed near a wall and <Pe_S> values are high. An explanation of this is that the anisotropic diffusivity migration only affects the distribution near the center of the channel in high <Pe_S>, as discussed in the rod migration theory [16-18]

4. DISCUSSION

As shown in Fig. 3 and Fig. 4, although rods and spheres have the same $D_\perp$ and D_O, they can have different R_M from R_S in FFF separation. Besides the difference of the

steric inversion between rods and spheres, identified by Phelan and Bauer [8], we have shown that the local orientation effect and the rod migration effect can also make the difference among the retention ratios. We will discuss how to characterize the conditions where each effect is dominant.

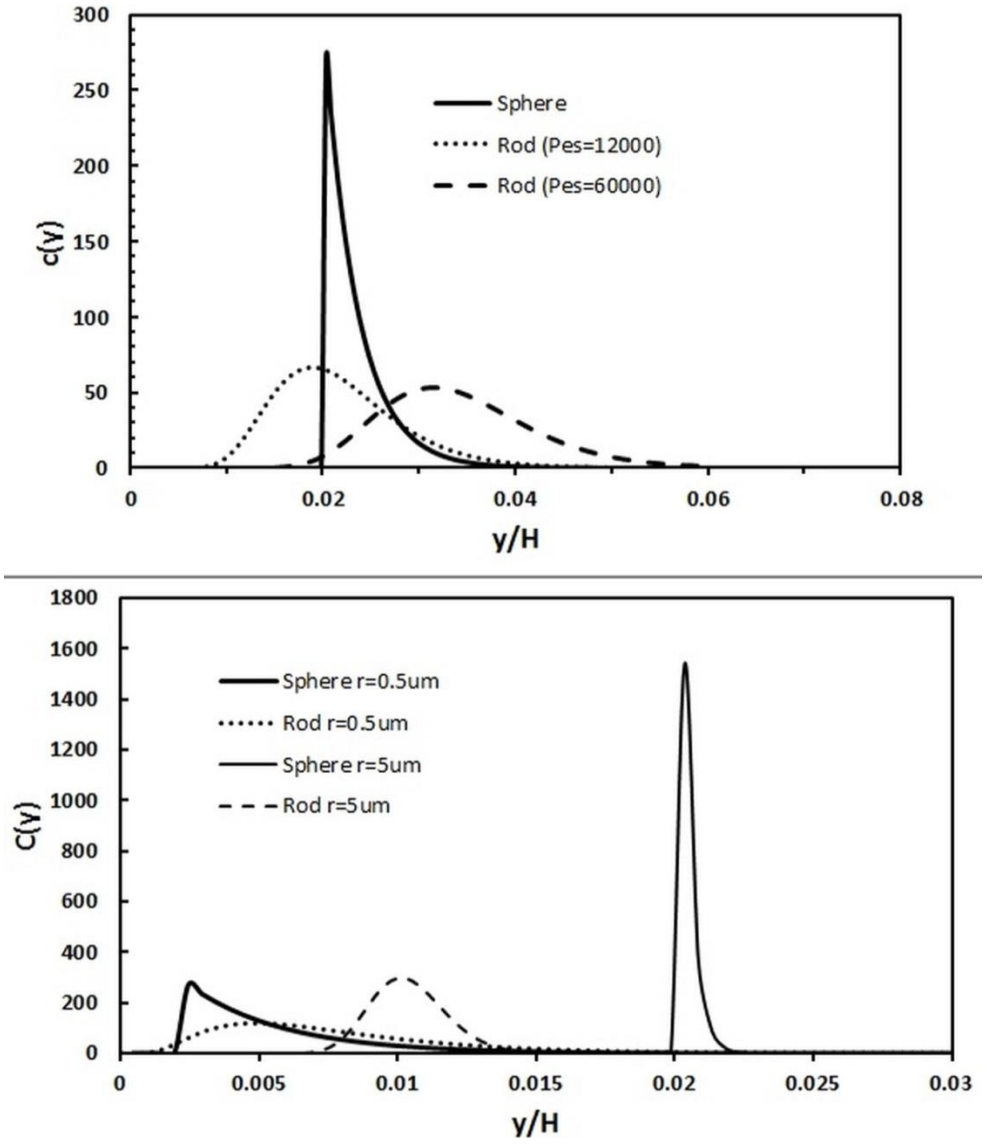

Figure 4. Concentration profiles of rods with A=100 and spheres in Fl-FFF: A) Pe_X=12000 and 60000, U_x=5×10^{-8} m/s, r_{eq}=5 μm, and B) Pe_X=60000, U_x=5×10^{-7} m/s, r_{eq}=0.5 μm and 5 μm.

We introduced the following new Peclet numbers based on the 'cross' flow rate for 'spheres' and 'rods', respectively:

$$Pe_{CS} = \frac{U_x r_{eq}}{D_O}, \text{and} \quad Pe_{CR} = \frac{U_x d}{2D_\perp} \tag{22}$$

The steric inversion of a sphere happens around Pe_{CS}~1, by reinterpreting the analysis by Phelan and Bauer [8]. Likewise, analyzing the results of R_R in Fig. 3.C can easily find that the steric mode of rods becomes dominant when Pe_{CR}>>1 as well as there is no migration. Additionally, the effect of the lift-hyperlayer mode of rods becomes obvious and results in larger R_M than R_R around $\langle Pe_S \rangle$ >1200, as predicted in the rod migration theory [16-18].

For the condition of Pe_{CS}>1 and $\langle Pe_S \rangle$ <1200, the steric mode of spheres becomes dominant so that spheres are eluted faster (R_S>R_M). However, when both the steric mode of spheres and the lift-hyperlayer mode of rods becomes effective for Pe_{CS}>1 and $\langle Pe_S \rangle$ >1200, there is a cross-over between R_S and R_M, as shown in Fig. 3.C. We discovered that this cross-over can be characterized by the ratio between $\langle Pe_S \rangle$ and Pe_{CS}, which are characterizing each mode. As shown in Fig. 5, the cross-over in Fig. 3.D closely matches the point where $\langle Pe_S \rangle / Pe_{CS} = 9\ln(2A)\langle v \rangle L/U_x w$ reaches approximately 2400. This ratio seems to characterize how much stronger the rods migrate away from a wall against being pushed towards the wall by the cross flow. We guess that the value 2400 is related to the order of magnitude of $\langle Pe_S \rangle$=1200, where the lift-hyperlayer becomes effective.

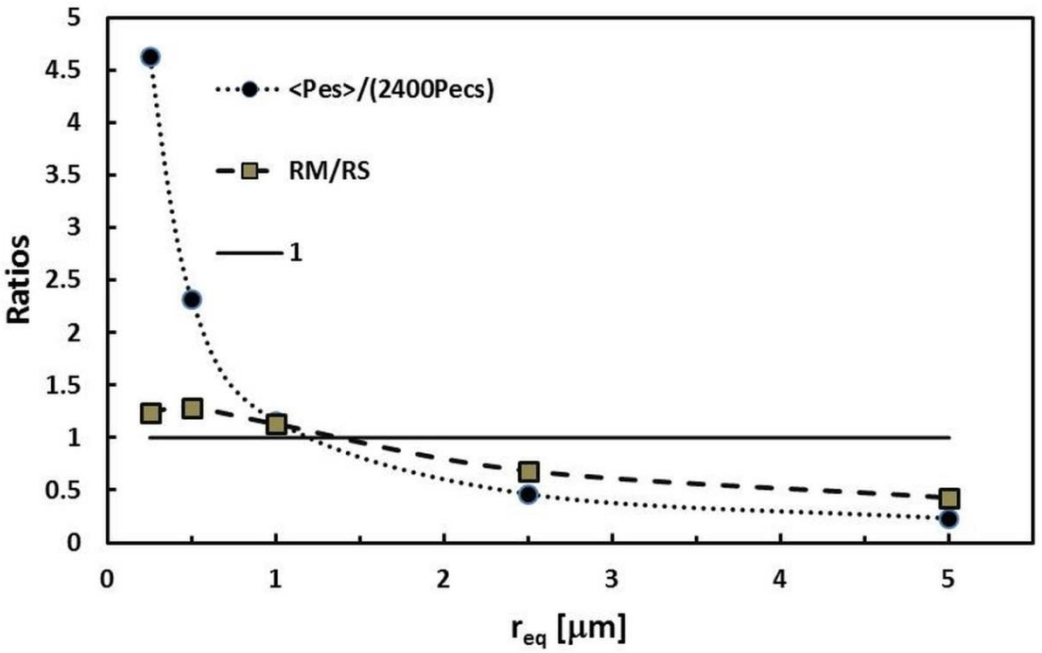

Figure 5. Identification of the cross-over of lift/steric mode by $<Pe_S>/(2400Pe_{CR})$ and R_M/R_S as a function of r_{eq} for the condition in Fig. 3.D. Ratios lower than 1 indicates that the steric mode is dominant.

For the normal mode only the condition of $Pe_{CS}<1$ and $<Pe_S>$ <1200, only the orientation effect, causes slightly larger R_M than R_S due to the non-zero $<<p_x^2>>$. Using this result, the length estimation of SWNTs by Chun [7], which assumed only the aligned configuration, can be improved. Based on our model, the lengths of SWNT are calculated to be 40% longer than the results from the assumption of the aligned configuration. However, the lengths measured by light scattering were shorter than the lengths evaluated from the assumption [7]. Additionally, the Brownian dynamics simulation also showed that the elution of spheres was slightly faster than that of rods for normal mode [8]. As already discussed by Phelan and Bauer [8], this discrepancy is conjectured to be attributed to how to deal with the dynamics of rods contacting with a wall. We can claim

that the discrepancy is at least not due to the local orientation or the migration. Further studies on Brownian dynamics simulation considering more rigorous modeling of interaction between rods and a wall, including the comparison with the rod steric correction [9], is required to resolve this issue. Experimental confirmation based on rodlike particles with the well-characterized length must be accompanied, too.

5. CONCLUDING REMARKS

We investigated the FFF separation of rods and spheres which have the same $D_{\perp}=D_O$. Previous studies [7,8] are based on the assumption that rods are aligned in the axial flow direction and the rods and spheres with $D_{\perp}=D_O$ show the same dynamic behavior for normal mode. However, our study considered the local orientation and included the rod migration for more rigorous analysis. The results have shown that separation behaviors of rods and spheres can be different according to the FFF conditions.

We characterized the conditions where each mode becomes dominant and identified the separation behavior in each condition. Rods will have the smaller elution time for the case of $Pe_{CS}<1$ and $\langle Pe_S\rangle >1200$ as well as the case of $\langle Pe_S\rangle / Pe_{CS}>2400$, where the lift-hyperlayer mode of rods is dominant. Rods are also predicted to be eluted faster, but only slightly, for the case of $Pe_{CS}<1$ and $\langle Pe_S\rangle <1200$. This is because the normal modes for both spheres and rods are dominant but the orientation effect slightly increases the diffusivity of rods. The elution of spheres will happen earlier for the case of $Pe_{CS}>1$ and $\langle Pe_S\rangle <1200$ as well as the case of $\langle Pe_S\rangle / Pe_{CS} <2400$, where the steric mode for spheres is dominant.

The theoretical analysis in this study can be used for the advancement of the shape separation of micro/nanoparticles using FFF. Examples include the design of the shape separation methods, the correction to length characterization of rodlike particles, and the interpretation/prediction of the experimental observations. Further simulation and experimental studies must be accompanied for the improvement as well as the clarification of the discrepancy from the previous studies [7,8,10].

APPENDIX

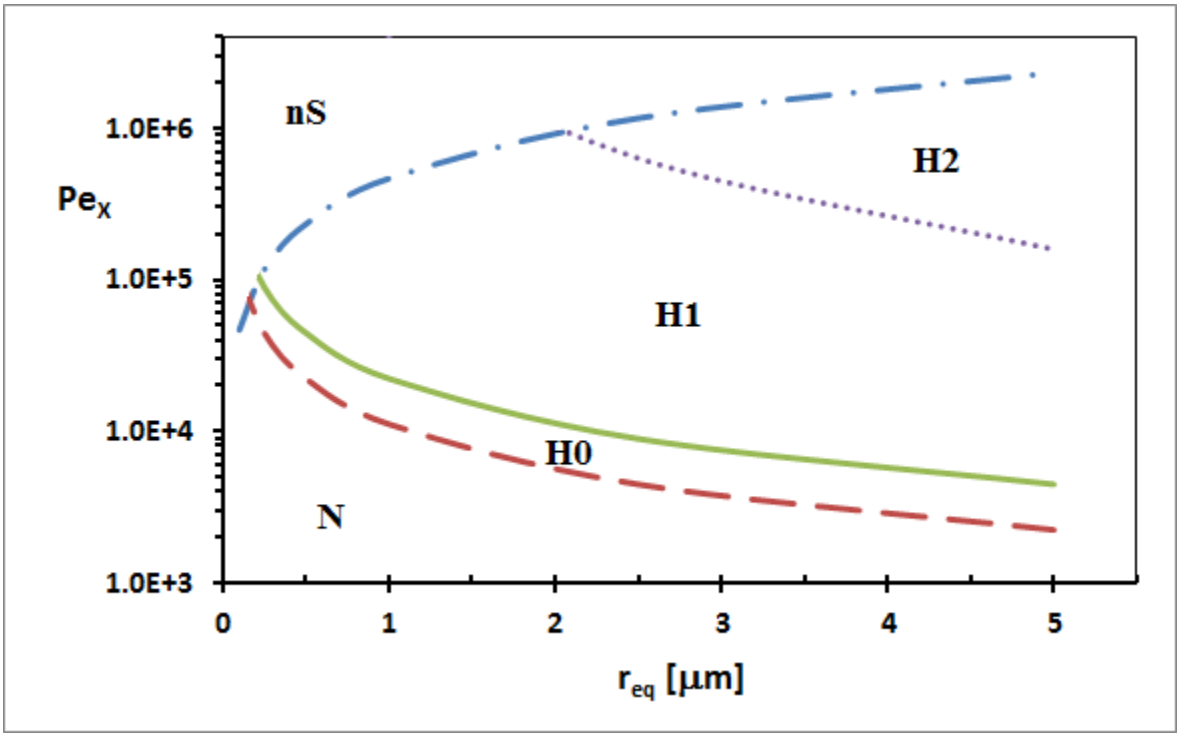

Figure A.1. Pe_X-r_{eq} diagram indicating the dominant separation modes of a rod with A=10 with varying Pe_{CS}.

- Region nS: non-Stokes flow condition
- Region N (Pe_{CS}<1 and <Pe_S> <1200): normal mode condition
- Region H (<Pe_S> >1200): lift-hyperlayer mode condition with sub-regions of
  - Region H0 (Pe_{CS}<1 and 1200< <Pe_S> <2400)
  - Region H1 (Pe_{CS} =1 and 2400< <Pe_S> <4800)
  - Region H2 (Pe_{CS} =2 and <Pe_S> >4800).

In section 4, we discussed the conditions where each mode is dominant in terms of Peclet numbers. In Fig. A.1, each separation criterion for a rod with A=10 is indicated on a diagram in terms of Pe_X and r_{eq} with varying Pe_{CS}.

Region nS: It corresponds to the condition where the Stokes flow assumption is not valid. In this region, the inertia becomes effective to the particle motion, which gives totally different dynamics from the scope of our study.

Region N (Pe_{CS}<1 and <Pe_S> <1200): It is the condition where normal mode is dominant.

Region H (<Pe_S> >1200): If the value of Pe_X is below the region nS and the above the region N, the lift-hyperlayer mode of a rod becomes effective in this region. However, if spherical particles of the same r_{eq} are mixed with rods, the separation behavior becomes dependent on the competition between the lift-hyperlayer mode of the rod and the steric mode of the sphere. Therefore, the region H can be divided into sub-regions according to the cross flow condition, which can be characterized with Pe_{CS}.

Region H0 (Pe_{CS}<1 and 1200< <Pe_S> <2400): In this condition, the rods in lift-hyperlayer mode are eluted faster than the spheres in normal mode.

Region H1 (Pe_{CS}=1 and 2400< <Pe_S> <4800): If the cross flow rate becomes higher, the faster elution of rods is possible only for high enough Pe_X to overcome the steric mode of the spheres. The border (green solid) line between the region H0 and the region H1 indicates the minimum value of Pe_X to prevail over the spheres under the cross flow of Pe_{CS} =1.

Region H2 (Pe_{CS}=2 and <Pe_S> >4800): As in Region H1, the value of Pe_X must be in Region H2, or above the purple dot line, to achieve the faster elution of rods than the spheres in steric mode under the cross flow of Pe_{CS}=2.

In summary, Fig. A.1. can be a guideline for the design of separation conditions of rods and spheres in FFF considering the lift-hyperlayer mode of rods.

BIBLIOGRAPHY

[1] Hough, L. A., Islam, M. F., Janney, P. A., Yodh, A. G. *Phys. Rev. Lett*. 2004, 93, 168102.

[2] Sharma, V., Park, K., Srinivasarao, M., *Mat. Sci. Eng. R* 2009, 65, 1-38.

[3] Guo, Z., Xu, F., Xu, L., Yang, D., *Chem. Commun*. 2011, 47, 4180–4182

[4] Runyon, J. R., Goering, A., Yong, K., Williams, S. K. R., *Anal. Chem*. 2013, 85, 940-948.

[5] Schimpf, M.E., Caldwell, K., Giddings, J.C., *Field-Flow Fractionation Handbook*, Wiley-Interscience, 2000.

[6] Moon, M. H., Kang, D., Jung, J., Kim, J., *J. Sep. Sci*. 2004, 27, 710-717.

[7] Chun, J., Fagan, J.A. , Hobbie, E.K., Bauer, B.J., *Anal. Chem*. 2008, 80, 2514-2523.

[8] Phelan Jr, F.R., Bauer, B.J., *Chem. Eng. Sci*. 2009, 64, 1747-1758.

[9] Beckett, R., Giddings, J.C., *J. Colloid Interface Sci*. 1997, 186, 53-59.

[10] Gigault, J., Cho, T.J., MacCuspie, R.I., Hackely, V.A., *Anal. Bioanal. Chem*. 2013, 405, 1191-1202.

[11] Nguyen, T.M., Gigault, J., Hackley, V.A., *Anal. Bioanal. Chem*. 2013, online issn 1618-2650.

[12] Gajdos, L.J., Brenner, H., *Sep. Sci. Tech*. 1978, 13, 215-240.

[13] Hijazi, A., Zoaeter, M., *Eur. Polym. J*. 2002, 38, 2207-2211.

[14] Chen, S. B., Jiang, L., *Phys. Fluids* 1999, 11, 2878-2890.

[15] Asokan, K., Ramamohan, T. R., Kumaran, V., *Phys. Fluid* 2002, 14, 75-84.

[16] Park, J., Bricker, J.M., Butler, J.E., *Phys. Rev. E* 2007, 76, 040801.

[17] Park, J., Butler, J.E., *J. Fluid Mech*. 2009, 630, 267-298.

[18] Park, J., *Dynamics of Suspensions of Rod-like Polymers with Hydrodynamic Interactions*, University of Florida Dissertation, 2009.

[19] Nitsche, J.M., Roy, P., *AIChE J*. 1996, 42, 2729-2742.

[20] Batchelor, G. K., *J. Fluid Mech*. 1970, 44, 419-440.

[21] Ausserre, D., Edwards, J., Lecourtier, J., Hervet, H., Rondelex, F., *Europhys. Lett*. 1991, 14, 33-38.

[22] Saintillan, D., Shaqfeh, E. S. G., Darve, E., *J. Fluid Mech*. 2006, 557, 297-306.

[23] Nitsche, L. C., Hinch, E. J., *J. Fluid Mech*. 1997, 332, 1-21.

[24] Schiek, R. L., Shaqfeh, E. S. G., *J. Fluid Mech.* 1997, 332, 23-39.

[25] Giddings, J.C., *Sep. Sci. Tech*. 1978, 13, 241-254.

VITA

Mehrdad Alfi was born in Tehran, Iran. He attended NOET (National Organization for Development of Exceptional Talents) and completed his high school education in 2007. He moved to University of Tehran and completed his Bachelor's degree in Chemical Engineering in 2012.

Mehrdad moved to United States of America in fall 2012 to pursue graduate studies in Chemical Engineering at Missouri University of Science and Technology. He will be graduating in May 2014 with a Master of Science degree in Chemical Engineering and will pursue a Ph.D. degree afterwards.